Self-similar transport in incomplete chaos

G. M. Zaslavsky
Courant Institute of Mathematical Sciences, New York University, 251 Mercer Street, New York, New York 10012 and Physics Department, New York University, 4 Washington Place, New York, New York 10003

D. Stevens and H. Weitzner
Courant Institute of Mathematical Sciences, New York University, 251 Mercer Street, New York, New York 10012
(Received 3 May 1993)

Particle chaotic dynamics along a stochastic web is studied for three-dimensional Hamiltonian flow with hexagonal symmetry in a plane. Two different classes of dynamical motion, obtained by different values of a control parameter, and corresponding to normal and anomalous diffusion, have been considered and compared. It is shown that the anomalous transport can be characterized by powerlike wings of the distribution function of displacement, flights which are similar to Lévy flights, approximate trappings of orbits near the boundary layer of islands, and anomalous behavior of the moments of a distribution function considered as a function of the number of the moment. The main result is related to the self-similar properties of different topological and dynamical characteristics of the particle motion. This self-similarity appears in the Weierstrass-like random-walk process that is responsible for the anomalous transport exponent in the mean-moment dependence on t. This exponent can be expressed as a ratio of fractal dimensions of space and time sets in the Weierstrass-like process. An explicit form for the expression of the anomalous transport exponent through the local topological properties of orbits has been given.

PACS number(s): 05.45.+b, 47.52.+j, 05.60.+w, 47.53.+n

I. INTRODUCTION

When speaking about dynamical chaos, one has in mind that a particle exhibits some kind of random motion, so that the particle orbit can be represented by a random process. It is a major problem in the theory of chaos to specify this process. In early studies of chaotic systems it became clear that a Gaussian process could be considered as a fairly good approximation for many cases [1]. At the same time it was clear that chaotic motion of generic Hamiltonian systems is not ergodic and islands of stability form a finite measure fractal set in the phase space of a system. The islands induce more or less strong correlation effects and change the law of particle diffusion [2–7] (a review of many results can be found in [7]). One can conclude from these results that the stochastic process which describes a particle orbit is sensitive to the topology of the phase space and in particular to such fine topological objects as cantori [8,9,6]. It was shown in the works cited that particle transport for the standard map (or for a map similar to it) can be described by the diffusion equation of the Fokker-Planck-Kolmogorov type with a nontrivial diffusion coefficient $D(K)$ which depends on the critical parameter K characterizing the map. The so-called standard map describes a model of a perturbed rotator and the parameter K characterizes a level of perturbation. There is a strong chaos for $K \gg 1$ and the diffusion process is close to Gaussian. Diffusion occurs for $K > K_c = 0.914\ldots$ and there are fairly strong oscillations of $D(K)$ for $K - K_c$ not too large. The variation of $D(K)$ exemplifies the dependence of the diffusion process on the measure of islands, which is of the order $1/K^r$, with some exponent r of order one.

Hamiltonian chaos allows a wide variation of topology in phase space and correspondingly, a wide variation in transport possibilities can be imagined between the slow process such as Arnold diffusion [10] and the normal diffusion of Gaussian-like process. In many Hamiltonian systems of interest with chaotic orbits, the system is close to an integrable one. In such Hamiltonian systems chaos is "weak," which means that chaotic orbits are concentrated in small measure domains of phase space. Topological construction of the domains of weak chaos is very complicated and notions of "web" or "stochastic web" are often used to describe these domains. The discovery of the stochastic webs of different symmetries in low-dimensional Hamiltonian systems [11–13] shows that the problem of particle transport is more serious and more important in applications than one might have otherwise thought. It was shown in a set of publications [14–17] that transport through stochastic webs could be intrinsically non-Gaussian, i.e., anomalous. Such a transport can be characterized by a non-Gaussian time dependence of the moments of the particle displacement R,

$$\langle R^2 \rangle \sim t^{\gamma}, \quad t \to \infty , \tag{1.1}$$

with $\gamma \neq 1$. It can be superdiffusion $(1 < \gamma < 2)$ [15–17] or subdiffusion $(0 < \gamma < 1)$ [16,18]. Preliminary investigations of anomalous transport phenomena display the existence of long ballistic modes in particle orbits [14–17] for which γ is close to 2, and even superlong modes [16,19]. The portions of orbits with almost regular (i.e., almost nonchaotic) propagation were called flights and jets.

The expression (1.1), while describing the transport properties, arises from large scale (long-time) asymptotics. At the same time (1.1) can be considered to be a result of some small scale, i.e., local, properties of the system. From the dynamical point of view their origin could be fractal local properties of scattering [20], renormalization-group properties of resonances [21,22], nontrivial statistics of the Poincaré recurrences [23], or Hamiltonian intermittency (see examples in [13]). It was shown in [15,17] that the occurrence of flights depends on the topological properties of the system's phase portrait, namely on its symmetry and on the closeness of the system's parameters to their bifurcation values.

For several reasons it was supposed in [14–17] that anomalous transport (1.1) with $\gamma \neq 1$ correspond to the Lévy-flight-like random process [24]. The first reason was strictly formal: Lévy flights are described by the distribution function $p_n(x)$ of probability to have displacement x after the nth step of random walk, which has the asymptotic form

$$p_n(x) \sim \text{const} \times n / x^{1+\alpha}, \quad n \to \infty , \tag{1.2}$$

where $0 < \alpha < 2$. The power tail indicates the absence of a characteristic size, the intermittency or dominance of large length steps, and the self-similar property of the moments of p_n. It was mentioned in [14–17,19] that particle orbits can be trapped in regions in the vicinity of islands of stability. Such trappings create long flights in the perpendicular direction to the islands, and such flights may be responsible for the powerlike tails in the distribution function. The second reason was based on the results of works [25–27], in which the connection of α to the fractal dimension of a space of the particle random walk was established and a Lévy process was used to describe the Richardson law for self-similar particle diffusion in a turbulent fluid. The third reason was based on the fractal properties of the islands' topological distribution in the phase space of a particle. If trappings or flights are significant for a particle orbit, then the fractal structure of the areas of trappings should induce a self-similar asymptotic form for the particle's displacement distribution function. The fourth reason was well elaborated for Lévy-like processes, the idea of fractal time [29,30] which gives a freedom to operate with a dynamical orbit with fractal structure in both space and time. Corresponding phenomenological kinetic equations were proposed in [16] (integral equations) and [31] (fractional Fokker-Planck-Kolmogorov equations). All these reasons may be considered as qualitative arguments which might lead one to find the correct form for the stochastic process of a particle wandering in dynamical chaos. The only observations that seem fairly reliable are the strong correlations between trappings near the boundary layer of an island and the occurrence of flights [17,19,28], and dependence of the exponent γ in (1.1) on a control parameter of the system, i.e., on the topology of the system's phase space [15].

This article is devoted to a detailed study of properties of the wandering process in the case of anomalous transport for an appropriate model of particle dynamics. The model describes a Lagrangian particle advection in a three-dimensional stationary flow with hexagonal plane symmetry. The flow was introduced in [12] (see also [13,14]) as a generalization of the Arnold-Beltrami-Childress (ABC) flow [32]. The great interest in such models originated with studies of the fast magnetic dynamo problem and of certain problems in convection (see [13]). To simulate anomalous transport of the form (1.1) and presumably with distribution (1.2) one needs long-term computations with high accuracy and large statistics of orbits. The model of hexagonal symmetry flow is appropriate because of its clear and well observable anomalous transport properties (see discussion in Sec. II). Our aim was to demonstrate the existence of different nontrivial features in a particle statistics rather than to carry out a detailed study, a much more difficult and lengthy problem. We believe that our results make obvious the proposition that Hamiltonian dynamical chaos is generically non-Gaussian. On occasion, the asymptotic properties of the dynamical chaos are close to the Lévy-like process with self-similarity. However, our concluding discussion shows the origin of more complicated probabalistic structure than a simple Lévy process for dynamical chaos.

In a simplified form the main result can be formulated as a possibility to predict in an explicit form the transport exponent γ in Eq. (1.1) or, better, the exponent μ in the equation

$$\langle |R| \rangle \sim t^{\mu}, \quad t \to \infty , \tag{1.3}$$

from the local topological properties of the phase space of a system. Specifically $\mu = \beta/\alpha$, where β is responsible for the time-behavior process near islands and is equal to the fractal dimension of this process, and α is responsible for the phase-space structure of orbits near islands and is simply connected to the fractal dimension of the islands-around-islands set. It is shown that β can be expressed through the Lyapunov exponents and α can be expressed through the island areas. Under some restrictions one can expect that α and β are universal constants and therefore there are universal anomalous transport exponents.

II. DESCRIPTION OF THE MODEL

We consider the motion of a Lagrangian particle in a stationary divergence-free velocity field $\mathbf{v} = \mathbf{v}(x,y,z)$, div $\mathbf{v} = 0$. Its motion is governed by the simple equation

$$\frac{d\mathbf{r}}{dt} = \mathbf{v}(\mathbf{r}) , \tag{2.1}$$

and its orbits coincide with streamlines of the vector field $\mathbf{v}$. Our flow field also satisfies the Beltrami property

$$\mathbf{v} = \text{curl } \mathbf{v} , \tag{2.2}$$

so that if one replaces the velocity field $\mathbf{v}$ by the magnetic field $\mathbf{B}$ then (2.1) characterizes the magnetic-field lines and (2.2) shows that the magnetic field is force free. In [12] a general q-fold symmetric Beltrami field $\mathbf{v}$ was constructed (the so-called Q flow), which gives the ABC flow for $q = 4$ and hexagonal flow for $q = 3$ or 6. For the latter case we have

$$\mathbf{v}=\left[-\frac{\partial\psi}{\partial y}+\epsilon\sin z,\frac{\partial\psi}{\partial x}+\epsilon\cos z,\psi\right], \tag{2.3}$$

where ϵ is a parameter of the system and ψ is a two-dimensional stream function with hexagonal symmetry in the (x,y) plane,

$$\psi=\cos x+\cos\frac{x+\sqrt{3}y}{2}+\cos\frac{x-\sqrt{3}y}{2}. \tag{2.4}$$

Equations (2.3) and (2.4) determine a three-dimensional periodic flow in space for which solutions of Eq. (2.1) can be chaotic.

It was shown in [12,13] that for arbitrary $\epsilon\neq 0$ there

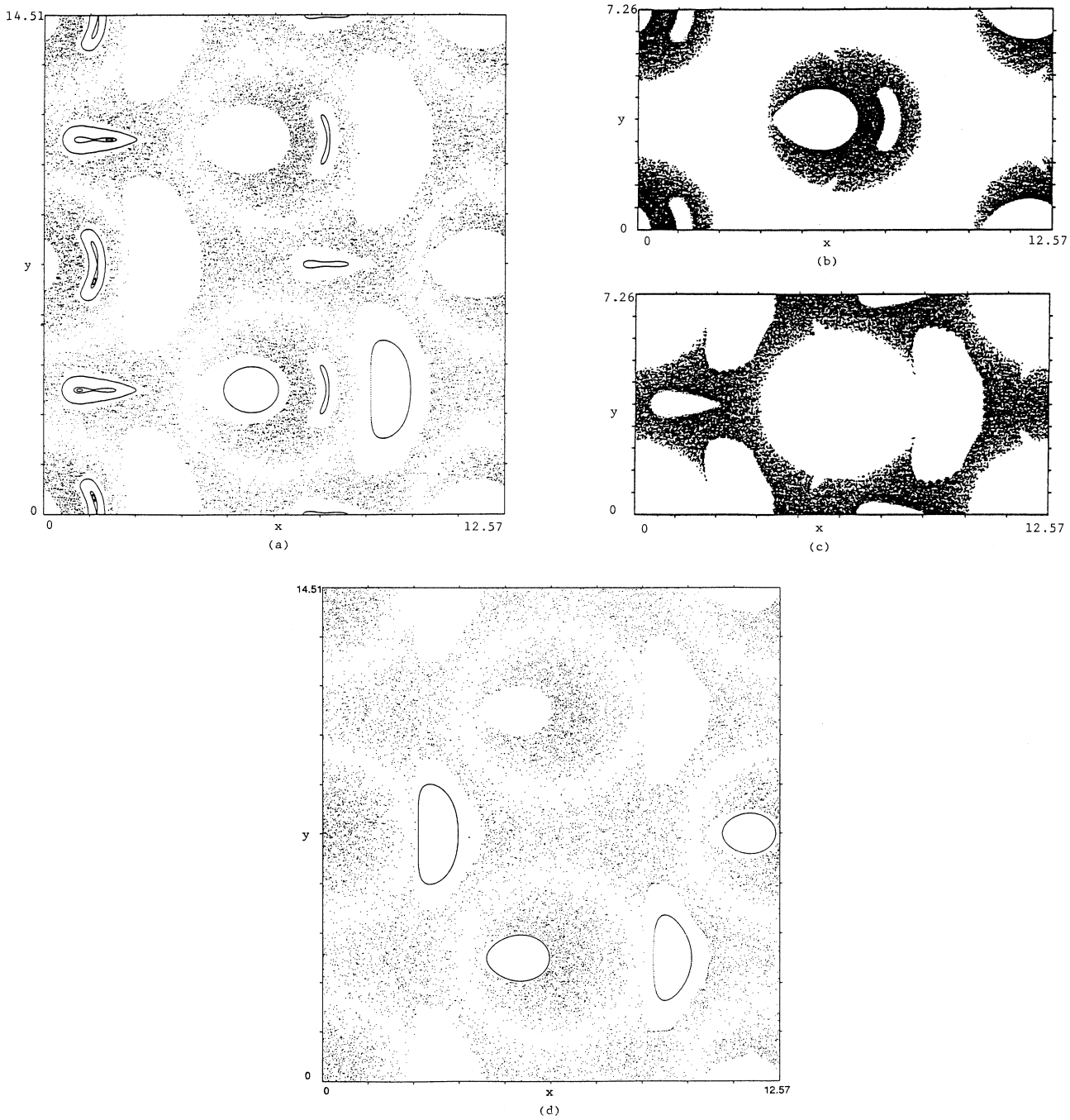

FIG. 1. Poincaré sections $z=0\ (\mathrm{mod}2\pi)$ of the particle orbit in the hexagonal flow for two values of ϵ: in (a), (b), and (c) $\epsilon=2.3$ and in (d) $\epsilon=2.9$. (a) displays two periods in y and one period in x; there are several regular orbits and one chaotic orbit, which undergoes propagation along z in both positive and negative directions. (b) and (c) display one period in x and one period in y for the same chaotic orbit as in (a) but for the (b) positive or (c) negative directions of propagation only. (d) is the same as in (a) but for $\epsilon=2.9$.

exists a connected infinite area of chaotic motion, called a stochastic web. The web looks like a connected net of channels inside of which particle orbits are chaotic. The characteristic value of the channel's diameter can be considered as the web width which is of order ϵ for small ϵ and of order 1 for $\epsilon > 1$.

Figure 1(a) shows a section of the stochastic web for $z = \text{const}$. A full stochastic web section comes from the doubly periodic continuation of the plot. Instead of three-dimensional imaging of the web it is convenient to look at its Poincaré sections for $z = \text{const} \pmod{2\pi}$. The model (2.1) has a Hamiltonian formulation for arbitrary ψ [13], but for our purposes the use of noncanonical variables (x,y) is satisfactory and simpler. Figures 1(b) and 1(c) present two maps: (b) displays an orbit inside the web which cross the plane $z=0$ in the positive z direction, and (c) displays the crossings in the negative z direction. Their superposition and periodic extension gives the web of Fig. 1(a). Figure 1(d) presents the Poincaré section of the stochastic web similar to Fig. 1(a) but for a different value of ϵ. The difference between Fig. 1(a) and Fig. 1(d) is in their topological structure. Two kinds of islands present in Fig. 1(a) are absent in Fig. 1(d), and it is just these islands which are responsible for long flights.

The orbit of a Lagrangian (passive) particle is a solution of the Eq. (2.1) $\mathbf{r} = \mathbf{r}(t;\mathbf{r}_0)$ satisfying the initial condition $\mathbf{r}_0 = \mathbf{r}(0;\mathbf{r}_0)$. At the same time $\mathbf{r}(t,\mathbf{r}_0)$ represents the streamline which starts from a point $\mathbf{r}_0$. We refer to the (x,y) plane as the phase plane even though x and y are not canonically conjugate, since there exists transformation of parameter $t \to \tau$,

$$d\tau = v_z dt = \psi dt \ , \tag{2.5}$$

for which x and y are canonically conjugate with an appropriate Hamiltonian [12]. The transformation (2.5) is singular at some points and must be used carefully at these points, but we do not need to use any of its properties.

Although the full phase portrait of the system (2.1) and (2.2) must be represented on a three-dimensional torus [see Fig. 1(a)], we examine the Poincaré plot of the orbit in the (x,y) plane corresponding to $z = 0 \pmod{2\pi}$. We define the displacements of a particle during a time t as

$$X = x(t) - x_0, \quad Y(t) = y(t) - y_0 \ . \tag{2.6}$$

We also introduce the probability distribution function of the position coordinates $p(x,y,t)$ with the normalizing condition

$$\int p(x,y,t)\,dx\,dy = 1 \ , \tag{2.7}$$

and we introduce the moments of $p(x,y,t)$ corresponding to (2.6),

$$\begin{aligned} \langle |X|^m \rangle &= \int |x(t) - x_0|^m p(x,y,t)\,dx\,dy \ , \\ \langle |Y|^m \rangle &= \int |y(t) - y_0|^m p(x,y,t)\,dx\,dy \ . \end{aligned} \tag{2.8}$$

The values of $\langle |X|^m \rangle$ and $\langle |Y|^m \rangle$ for large m depend essentially on the asymptotic behavior of $p(x,y,t)$ for large x and y. Gaussian or Gaussian-like distributions have exponentially decaying tails for $x,y \to \infty$ which render the expressions (2.8) integrable for any order m of the moments. In the case of anomalous transport the tail in $p(x,y,t)$ for large x,y is powerlike, leading to a large contribution from the tail to the integrals (2.8) and a strong growth of the moments for large m, and finally nonexistence of the moments for m large enough.

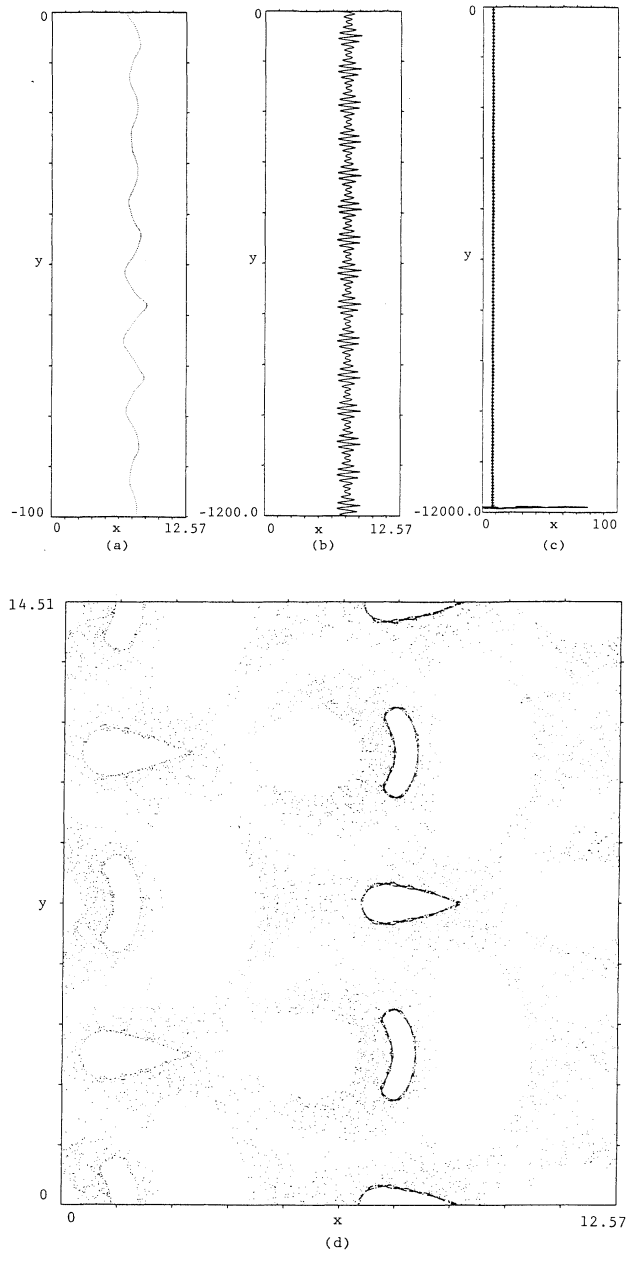

FIG. 2. A Lévy-like flight in y for $\epsilon = 2.3$ shown for different time intervals (a), (b), and (c). The Poincaré section (d) shows an almost periodic structure for different time intervals in (a), (b), and (c) and an escape from the flight in (c) after a very long time. All dots in (d) belong to the same flight: the dark part of the plot corresponds to the flight while all other dots are related to the part of the orbit which corresponds to the escape from the flight.

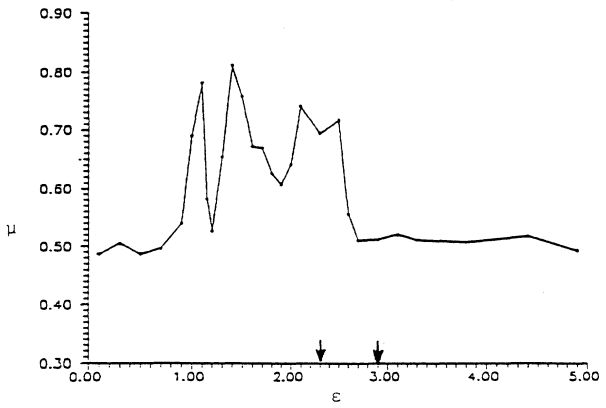

FIG. 3. Exponent of diffusion vs control parameter ϵ. Arrows indicate $\epsilon=2.3$ and 2.9, for anomalous and normal diffusion, respectively.

The possibility of the anomalous (non-Gaussian) situation dictates the way to study the orbits (solutions) of the system (2.1), (2.3), and (2.4). It was shown in [15,19] that chaotic orbits can have almost regular parts (flights) when a particle sticks fast in a boundary layer of islands. An example of a flight is shown in Fig. 2. The flight appears to be propagation along y direction [Figs. 2(a)–2(c)]. The same flight can be displayed on the three-dimensional torus due to the periodicity of the hexagonal flow model [see Eqs. (2.3) and (2.4)]. The two-periodic closure in the x direction in Fig. 2(d) shows clearly through the darker regions the stickiness of the flight to islands' boundaries.

Generic Hamiltonian systems with chaotic dynamics may have islands in the phase space and consequently may have flights. Nevertheless the statistics of the flights depends on various control parameters. One can introduce an exponent μ [see also (1.3)],

$$\langle R \rangle = \text{const} \times t^{\mu} \quad (t \to \infty) , \tag{2.9}$$

where $R=(X^2+Y^2)^{1/2}$, and consider the dependence $\mu=\mu(\epsilon)$ for the model used here, Fig. 3 [15]. Arrows show two values of $\epsilon=2.3$ (anomalous transport) and $\epsilon=2.9$ (normal diffusion), both of which we consider below. The advantage of the present model is existence of both normal and abnormal transport; we can use the plot in Fig. 3 to choose between them and compare them.

III. NUMERICAL SIMULATION DESCRIPTION

We have mentioned in the introductory part that it is desirable to have high accuracy simulation in order to get good statistics of the long flights. We employ a sixth-order Taylor expansion of the orbit to calculate time evolution of x,y,z for each step Δt. The formulas for higher-order time derivative were computed with a symbolic algebra program PFSA [33].

The time step Δt was selected by choosing as large a value as possible which gives good accuracy. First, we defined a standard test evolution, starting at (x_0,y_0,z_0) and running for total time $t=20$. This standard was computed with quadruple precision with both the above Taylor expansion method and with a fourth-order Runge-Kutta method. The sixth-order method attained 17-decimal-place accuracy with $\Delta t=0.000\,312$, and the Runge-Kutta method attained 11-decimal-place accuracy with this same Δt.

Using the accurate answer we did several double precision computations of x,y,z at $t=20$ using the Taylor expansion method with many values of Δt, then a value of 0.01 was selected, which gives an accuracy of 8 decimal places. With the Runge-Kutta method $\Delta t=0.001\,25$ is needed to get the same accuracy. The running time with the Taylor method and $\Delta t=0.01$ is 0.67 seconds, and with the Runge-Kutta method with $\Delta t=0.001\,25$ the time is 2.13 seconds. The corresponding accuracy with the Runge-Kutta method with the selected $\Delta t=0.01$ is 5 decimal places.

All the comparisons between different methods and values of Δt were computed for a typical chaotic orbit with $\epsilon=2.3$ (see Fig. 1).

IV. ANOMALOUS DISTRIBUTION FUNCTION

We introduce the distribution functions $P(x,t_0)$ or $P(y,t_0)$, which are calculated as follows. Let Δt be the time length of a step and Δx or Δy be sizes of bins along x or y directions. Then the normalized number of visits in a bin with coordinate x in the interval $(x,x+\Delta x)$ during a time interval $(0,t_0)$ is $P(x,t_0)$. $P(y,t_0)$ is defined similarly. Clearly $P(x,t_0)$ and $P(y,t_0)$ are histograms, depending on the choice of Δx, Δy, and Δt.

Figure 4 presents two distribution functions calculated by averaging the distribution functions of 400 different orbits. Plots in Figs. 4(a) and 4(b) correspond to $\epsilon=2.9$. The dashed curve is the best approximating Gaussian. The special plot of the wings of the distribution function [Figs. 4(c) and 4(d)] confirm their Gaussian form at least for large time asymptotics, since $\log_{10}P(x,t_0)$ are linear functions of x^2 or y^2, respectively, except for very large values of x,y for which there are large fluctuations due to the finite value of t_0. Clearly, Fig. 4 indicates normal diffusion. Nevertheless, the behavior of $P(x,t_0)$ and $P(y,t_0)$ for small x,y displays sharp peaks which are non-Gaussian. We discuss this feature further in Sec. IX.

A different situation occurs for $\epsilon=2.3$ for which anomalous transport occurs. Fluctuations are stronger in this case and averaging was performed over 620 orbits with $t_0=10^4$ for each. The corresponding distributions $P(x,t_0)$ and $P(y,t_0)$ are shown in Fig. 5. The wings of the distribution functions have power-law dependence, as shown by Fig. 6, in which we present a plot of $\log_{10}P$ versus the logarithm of the coordinate and a plot of $\log_{10}P$ versus the square of the coordinate for comparison. A rough estimate of the exponents

$$P(x,t_0)\sim 1/x^{1+\alpha_x}, \quad P(y,t_0)\sim 1/y^{1+\alpha_y} \tag{4.1}$$

gives

$$\alpha_x \approx \alpha_y \approx 3 . \tag{4.2}$$

There is not enough accuracy in our computations to identify anisotropy in the x and y directions or to obtain

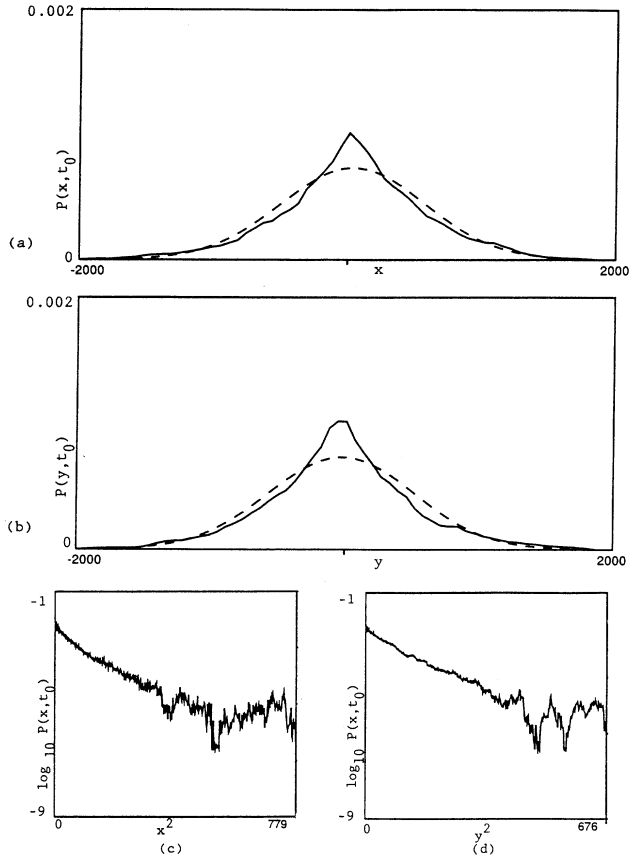

FIG. 4. Normalized distribution functions (a) $P(x,t_0)$ and (b) $P(y,t_0)$ for the case of $\epsilon=2.9$. (c) $\mathrm{Log}_{10}P(x,t_0)$ vs x^2 and (d) $\log_{10}P(y,t_0)$ vs y^2 for large t_0 exhibit the Gaussian character of P. The large fluctuations at the end of the plots are due to the lack of statistics at large distances.

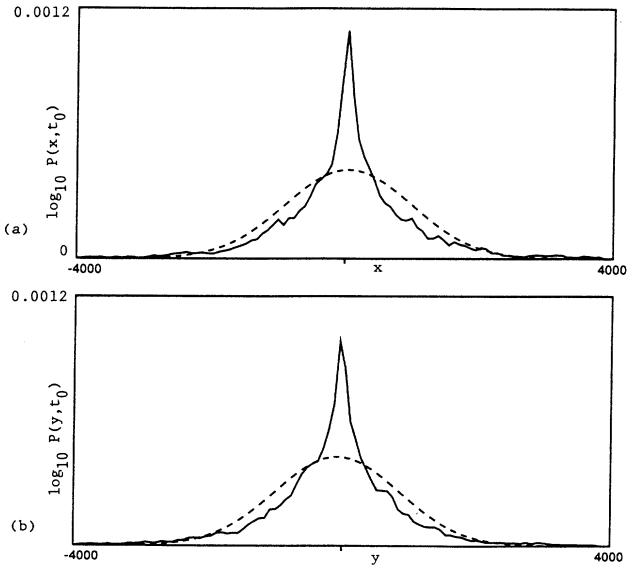

FIG. 5. The same as in Figs. 4(a) and 4(b) but for the anomalous diffusion case $\epsilon=2.3$. The dashed curve is the corresponding Gaussian with the same standard deviation and mean.

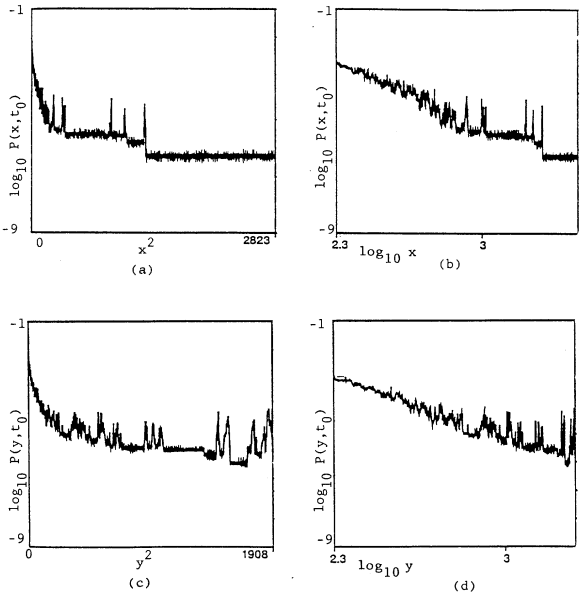

FIG. 6. An analysis of the distribution tails for the anomalous diffusion case $\epsilon=2.3$. (a) and (b) exhibit plots of $\log_{10}P$ vs x^2, y^2. (c) and (d) exhibit plots of $\log_{10}P$ vs $\log_{10}x$, $\log_{10}y$.

α_x or α_y accurately. An important feature of the distribution function in the anomalous case of $\epsilon=2.3$ can be seen if we plot $P(x,t_0)$ and $P(y,t_0)$ after averaging over only 100 orbits and with higher resolution (small bin size) (Fig. 7). There are many peaks and each peak corresponds to a different flight. It is just these flights which cause the orbits to stick fast at some coordinates, enormously enhancing fluctuations and changing asymptotics for the large coordinate values.

Another way to find anomalous properties of the distribution functions $P(x,t_0)$ and $P(y,t_0)$ is to look at the

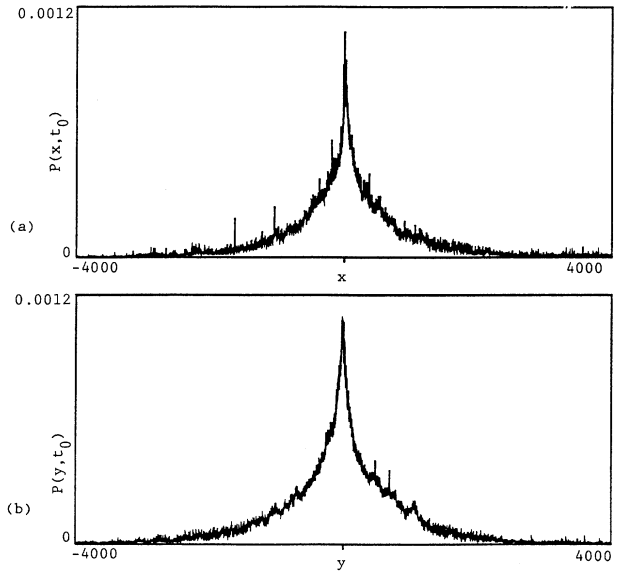

FIG. 7. Nonsmoothed histogram of the distribution functions in Fig. 5 for the case of anomalous diffusion.

moments (2.8) and the dependence of the moments on the moment number m. Due to the powerlike asymptotic law (4.1) the moments grow much faster as m increases than the growth for the Gaussian form of the distribution function. Results of the corresponding calculations are given in Fig. 8. All curves represent $\log_{10}\langle |X|^m \rangle$ vs m for the interval of m (0,10). The curve 1 corresponds to the distribution $P(x,t_0)$ in Fig. 4(a) for $\epsilon=2.9$, which we supposed to be close to the Gaussian for large x. The dashed curve 2 corresponds to the Gaussian approximation for the same $P(x,t_0)$ [see the corresponding dashed curve in Fig. 4(a)]. The Gaussian distribution has been adjusted by taking equal second-order moments for Gaussian distribution and for the calculated one. Within the plotted range the curves 1 and 2 are very close. The curve 3 corresponds to the anomalous distribution $P(x,t_0)$ in Fig. 5(a) for $\epsilon=2.3$. There is an obvious strong discrepancy between curves 1 (or 2) and 3, a result of powerlike wings for a distribution function exhibiting anomalous diffusion.

Some additional information about the role of flights in creating powerlike tails of the distribution function appears if one reduces the accuracy of computations. Errors from roundoff and lack of precision may generate additional randomness in the dynamics and may, correspondingly, in its turn, reduce the length of flights. Shorter flights reduce the powerlike dependence of the tail of the distribution function and reduces the growth of the higher moments as m increases. Curve 3 in Fig. 8 corresponds to the sixth-order computations after averaging over 620 orbits. Curve 4 in Fig. 8 corresponds to the same initial conditions but with orbits computed by the fourth-order Runge-Kutta method in single precision, and is closer to the normal distribution. This example demonstrates, in particular, the importance of computational accuracy for the study of anomalous transport.

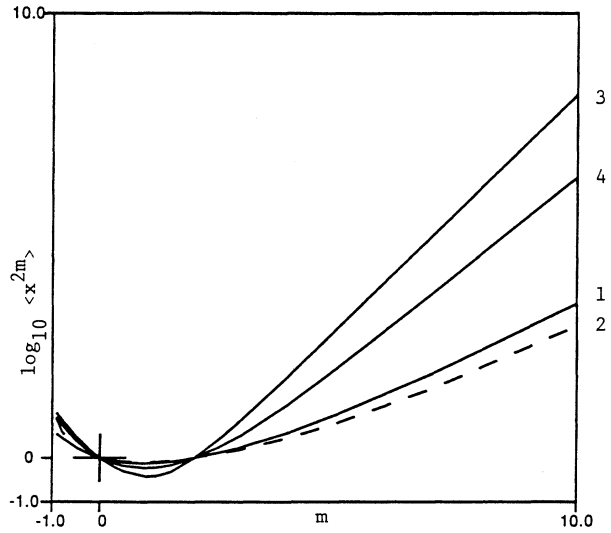

FIG. 8. Plot of the dependence of the moment of order m on m. Curve 1 corresponds to $\epsilon=2.9$; curve 2 is for a Gaussian approximation of the curve 1; curve 3 is for the anomalous diffusion case $\epsilon=2.3$; and curve 4 is for a low precision computation of the previous case.

V. SELF-SIMILARITY OF TRANSPORT

The picture of the origination of flights, described above, is influenced by the increasingly fine structure of the island patterns in phase space and its specific properties. It was mentioned in [34] that in the neighborhood of a generic periodic orbit there are satellite elliptic orbits of smaller sizes and so forth. More precisely these satellite elliptic orbits are ordered forming a chain of islands around the main island [35]. This situation is known as "islands around islands" [36]. Its main feature is self-similarity, which gives a possibility to apply renormalization-group methods [36,37]. To make explicit the islands around islands picture for our problem we present a corresponding simulation in Fig. 9 where four generations of a parent island are shown. A dark region on the boundary strip of an island is the result of flights.

The method of class renormalization for islands around islands was proposed in [36]. Let us consider equations of motion (2.1) and their solution in the form

$$x=x(z;x_0,y_0,z_0),\quad y=y(z;x_0,y_0,z_0)$$

where (x_0,y_0) are "initial conditions" at $z=z_0$. Then one can introduce the mapping **T**, which is a shift operator generated by the solution of (2.1) corresponding to two consequent crossings of the plane $z=\text{const}\ (\text{mod}2\pi)$. A periodic orbit with a period q_i'/q_i (q_i',q_i are integers) is a fixed point of $\mathbf{T}^{q_i}$. By changing some parameter of the mapping **T** one can come to the first appearance of an islands chain encircling the periodic orbit of the frequency q_i'/q_i. Let the new frequency of smaller islands be

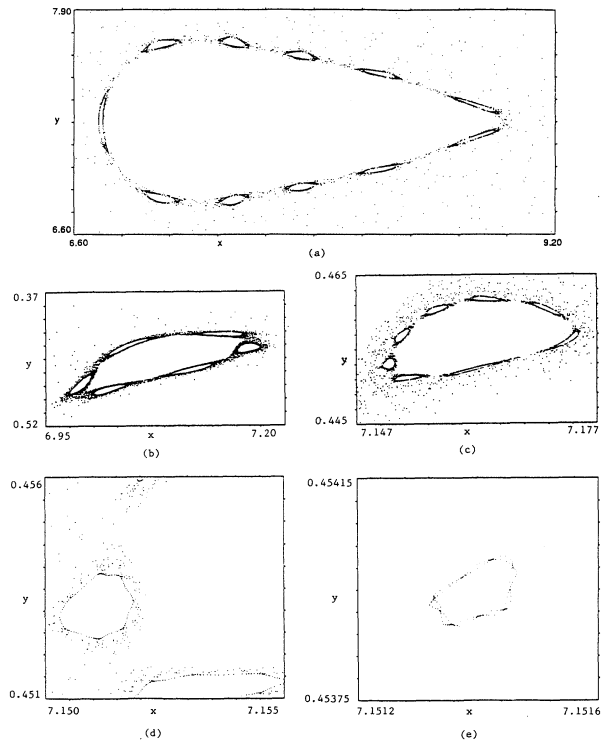

FIG. 9. Poincaré section for an orbit displays (a) the main island and (b)–(e) islands of four generations.

q'_{i+1}/q_{i+1}. We define the starting periodic orbit to be of order i, the next generated orbit is of order $(i+1)$, etc.

Let ΔI_s be the area of an island of order s. Computer simulation for a model of two-dimensional area-preserving mapping suggests the self-similarity [36]

$$\Delta I_s \sim C_I(\Delta\bar{I}_0)^{-s} , \tag{5.1}$$

with two appropriate constants C_I and $\Delta\bar{I}_0$. It was proposed in [36] that these constants are universal under some constrictions. Here we would like to go farther and introduce additional, related self-similarities, namely for the period of the last invariant curve that forms the boundary of the order $-s$ island,

$$T_s \sim C_T \bar{T}_0^s , \tag{5.2}$$

and for the Lyapunov exponents in the vicinity of the order $-s$ island,

$$\sigma_s \sim C_\sigma \bar{\sigma}_0^s \quad (\bar{\sigma}_0 < 1) , \tag{5.3}$$

where

$$\sigma = \lim_{t\to\infty, d(0)\to 0} \frac{1}{t} \ln[d(t)/d(0)] \tag{5.4}$$

and $d(t)$ is separation at the time instant t of two initially close orbits.

Table I confirms the statements of the self-similarities (5.1)–(5.3). The second column gives the value of q_s for the resonance of the order s. All other columns definitely show the exponential law of the correspondent value dependence on s. Column with n_s indicates the total number of order $-s$ islands. Their full area is

$$\delta I_s = n_s \Delta I_s . \tag{5.5}$$

Area of islands ΔI_s, period T_s, and growth times τ_s are taken in the same units as in the initial equations (2.3) and (2.4). The accuracy of the Lyapunov exponents σ_s is fairly low as extensive computations must be done to obtain the necessary average over different initial conditions. Nevertheless even such nonaveraged exponents display the exponential dependence on s. In particular the island area scaling parameter $\Delta\bar{I}_0 \sim 10^{-2}$ and is close to the one considered in [36].

The complex island structures just described influence the behavior of a particle trapped in the area in the vicinity of the islands boundary. A Markov-tree model was proposed in [38,39] to describe the transport or survival probability in such systems. In the next section another model will be proposed to describe the non-Gaussian distribution of the particle displacements.

VI. SELF-SIMILAR RANDOM WALKS

A formal description for the chaotic motion with flights is based on two conjectures. The first one is that an orbit may be conditionally determined based on the "regular" (short-scaled) parts and on the flights (long-scaled parts). A prevalence of one over another part defines a character of the long-time behavior asymptotics. The second conjecture is that the long-scaled part of flights has self-similar properties which determine the long-range asymptotics. Both of these conjectures are well confirmed by the previous simulation data.

In a simplified form the kinetic description can be considered as a sequence of jumps with self-similar distances. Time intervals between jumps are self-similar, too. More specification is necessary to get a formal equation.

The process when flights predominate can be described in a form of special cluster construction. For each order $-s$ islands introduce order $-s$ boundary layers. A particle rotates in such a layer with a weak instability, i.e., corresponding to the very small Lyapunov exponent σ_s and to the large escape time from the boundary layer. After escaping from one boundary layer of the order $-s$ the particle can be trapped into another order $-s'$ layer and so on. This process can be expressed also as passing through the turnstiles of cantori [36,38,39]. After switching from one layer to another the particle changes its action from the value δI_s to the value $\delta I_{s'}$. One can do coarse graining of the part of the motion which belongs to slow crossing of a boundary layer, and consider only the time $1/\sigma_s$ which is necessary to do this, and the "jump" ΔI_s of the action. A consecutive set of values $\{\Delta I_s, \sigma_s\}$ defines a flight cluster. Now the particle orbit can be described as a random walk along the flight cluster. Such a random walk is similar to the Weierstrass random walk [40,27], which is closely related to the Lévy flight process.

Consider the probability density $p(\xi)$ to do a step which changes the action of a particle by ξ, i.e., the action I becomes equal to $I\pm\xi$ after the step. The step may have an arbitrary value of S, so that

$$\xi = \delta I_s = C'_I(\delta\bar{I}_0)^{-s}, \quad \delta\bar{I}_0 = \bar{q}\Delta\bar{I}_0 , \tag{6.1}$$

corresponding to (5.5) and (5.1), and $\bar{q}$ is some average value of q_s (see Table I). The probability $p(\xi)$ to do any

TABLE I. Values of the last invariant curve period T_s, inverse Lyapunov exponent τ_s, and area of island δI_s for different orders $s=0, 1, 2, 3, 4$ of islands. Column n_s displays number of islands (i.e., order of resonances) in a form of the product where the last multiplier corresponds to the number of the last subislands set. Ratios T_{s+1}/T_s, τ_{s+1}/τ_s, and $\delta I_{s+1}/\delta I_s$ are given for convenience.

s	q_s	T_s	T_{s+1}/T_s	$\tau_s = 1/\sigma_s$	τ_{s+1}/τ_s	δI_s	$\delta I_{s+1}/\delta I_s$	n_s
0	1	65		4.8×10^3		1.2		1
1	11	347	5.37	12×10^3	2.5	0.039	0.032	1×11
2	6	2002	5.76	45×10^3	3.75	0.0071	0.182	$1\times11\times6$
3	8	13236	6.61	180×10^3	4.0	0.00050	0.07	$1\times11\times6\times8$
4	7	82402	6.23	$\sim360\times10^3$	2.0	0.000032	0.064	$1\times11\times6\times8\times7$

step of the value ξ (i.e., to have changing of the action of the value ξ) in a unit time is

$$p(\xi)=\text{const}\times\sum_s p_s\{\delta(\xi-\delta I_s)+\delta(\xi+\delta I_s)\}\ , \qquad (6.2)$$

where p_s is the probability density to do a step of the value $\pm\delta I_s$,

$$\delta(\xi)=\begin{cases}1, & \xi=0\\ 0, & \xi\neq 0\end{cases},$$

and the constant is determined by the normalization condition

$$\sum_\xi p(\xi)=1\ , \qquad (6.3)$$

where the sum over ξ runs over all available jumps $\{\delta I_s\}$. The crucial point in finding p_s is to use

$$p_s\sim\frac{1}{t}\ln[\Gamma_s(t)/\Gamma_s(0)]=\sigma_s\ , \qquad (6.4)$$

where $\Gamma_s(t)$ is the phase volume of a dynamical system in the order $-s$ boundary layer, if initially taken $\Gamma_s(0)$ [41]. A simple meaning of the (6.4) is that the probability to cross a stochastic layer, i.e., "to make a step" during the unit time, is proportional to the inverse time of mixing in the stochastic layer. This time $\tau_s=1/\sigma_s$ and can be taken from the corresponding column of Table I, and from (5.3),

$$p_s=\text{const}\times\bar{\sigma}_0^s\ .$$

It was mentioned above that computations of the average Lyapunov exponents is very difficult and accuracy of σ_s in Table I is very low. It is simpler to use a period T_s of the last invariant curve instead of the $1/\sigma_s$. Then one has from (5.2),

$$p_s=C_T/\bar{T}_0^s\ . \qquad (6.5)$$

The motivation to replace (6.4) by (6.5) is fairly clear although the justification is not trivial. Let us fix consideration on the order $(s-1)$ island. Then some effective perturbation creates a resonance of order s and correspondent set of q_s subislands. Such a perturbation has period T_s. Just this perturbation is responsible for the occurrence of the corresponding boundary layer, which can be considered as a stochastic layer induced by the perturbation. Moreover, for all known analytical examples the Lyapunov exponent in the stochastic layer is proportional to T_s (see many examples in [13]), i.e.,

$$\sigma_s=\text{const}/T_s\ , \qquad (6.6)$$

where the const is some number. This result is fairly natural because there are no other physical time scales which could characterize the island boundary layer. Hence the assumption is that the const in (6.6) does not depend on s strongly and this statement can be verified immediately from the correspondent columns of Table I which shows that there is a factor of about 2 in the relation

$$T_{s+1}/T_s\sim 2\tau_{s+1}/\tau_s\ .$$

The origin of the factor 2 may arise from the averaging procedure which must be done to get the actual Lyapunov exponents σ_s and which was not performed in our computations.

After substitution of (6.5) to (6.2) we get

$$p(\eta)=\frac{a-1}{2a}\sum_s a^{-s}\{\delta(\eta-b^s)+\delta(\eta+b^s)\}\ ,$$

with notations

$$\eta=\xi/C_I,\quad a=\bar{T}_0,\quad b=\delta\bar{I}_0\ . \qquad (6.7)$$

Now the problem has been reduced to the so-called Weierstrass random walk [40,27], and corresponding results can be used from [40]. The characteristic function of $p(\eta)$ is

$$p(k)=\sum_\eta e^{ik\eta}p(\eta)=\frac{a-1}{a}\sum_{n=0}^{\infty}a^{-n}\cos(b^n k)\ . \qquad (6.8)$$

Expression (6.8) for $p(k)$ has the form of the Weierstrass function, which explains the notion "Weierstrass random walk." From Table I it is seen that $a>1$ and $1/\mu_W<1$, where

$$\mu_W=\ln b/\ln a=\ln(\delta\bar{I}_0)/\ln\bar{T}_0\ . \qquad (6.9)$$

These conditions imply [42] that $p(k)$ is an everywhere continuous nowhere differential function. For small values of k, $p(k)$ satisfies

$$p(k)-p(0)=0(|k|^{1/\mu_W})\ , \qquad (6.10)$$

with the same exponent μ_W and with $p(0)=1$.

Our aim now is to make a connection between the self-similarity described above and the asymptotics for the mean displacement $\langle R\rangle$ in (2.9) or, more precisely, to find μ in (2.9) as a function of μ_W.

VII. RENORMALIZATION APPROACH

The special character of the Weierstrass function $p(k)$ permits the renormalization approach [27]. From (6.8) it follows that $p(k)$ satisfies

$$p(k)=\frac{1}{a}p(bk)+\frac{a-1}{a}\cos k\ . \qquad (7.1)$$

Using (7.1) and the Poisson summation formula or an alternative transformation (see [40,43] and generalization for the higher-dimensional case [44]), it was shown that $p(k)$ may be represented in the form

$$p(k)=p_h(k)+p_s(k)\ ,$$

where $p_n(k)$ is analytic in the neighborhood of $k=0$, and $p_s(k)$ is singular at $k=0$ and

$$p_s(k)=|k|^{1/\mu_W}Q(k)\ , \qquad (7.2)$$

where $Q(k)$ is periodic in $\ln k$ with period $\ln b$. There exist explicit expressions for $p_h(k)$ and $Q(k)$ which, for simplicity, we do not present here. Instead, a simplified derivation of the transport law will be given. The asymptotic behavior $k\to 0$ just corresponds to the asymptotic behavior $\eta\to\infty$, which is of interest to get the transport.

Let us return to the expression (6.6) for the probability density $p(\eta)$ to make a step of the length η. The probability density $P_n(\eta)$ to have the action η on the nth step satisfies the Markov equation

$$P_{n+1}(\eta)=\int_{-\infty}^{\infty}p(\eta-\eta')P_n(\eta')d\eta' . \tag{7.3}$$

By extracting $P_n(\eta)$ from the both sides of (7.3) one has

$$\begin{aligned}\Delta P_n(\eta)&\equiv P_{n+1}(\eta)-P_n(\eta)\\&=\int_{-\infty}^{\infty}\{p(\eta-\eta')-\delta(\eta-\eta')\}P_n(\eta')d\eta' ,\end{aligned} \tag{7.4}$$

where $\delta(\eta-\eta')$ is now the ordinary Dirac δ function. Introduce the k transform,

$$\begin{aligned}P_n(k)&=\int e^{ik\eta}P_n(\eta)d\eta ,\\p(k)&=\int e^{ik\eta}p(\eta)d\eta ,\end{aligned} \tag{7.5}$$

where for simplicity the last expression will be used instead of the discrete transform (6.8). Then (7.4) and (7.5) yield

$$\Delta P_n(k)=[p(k)-1]P_n(k) . \tag{7.6}$$

Using (6.10) and the property for $p(0)=1$ [see also (7.1) and (7.2)], we rewrite equation (7.6) in the form

$$\Delta P_n(k)=\text{const}\times|k|^{1/\mu_W}P_n(k),\quad k\to 0 . \tag{7.7}$$

We now pass to the case of n large so that $\Delta P_n/\Delta t$ can be replaced by the time derivative $\partial P/\partial t$ if Δt is one step time interval and n is associated with a continuous time. Then

$$\frac{\partial}{\partial t}|k|^{-1/\mu_W}P(k,t)=\text{const}\times P(k,t) ,$$

where the dependence on t is shown instead of the index n, or

$$\frac{\partial}{\partial t}\int dk\, e^{-ik\eta}|k|^{-1/\mu_W}P(k,t)=\text{const}\times P(\eta,t) . \tag{7.8}$$

Equations (7.7) or (7.8) are adequate to obtain the final answer on the asymptotic behavior of the particle transport. Using the asymptotic representation for $\eta\to\infty$ and performing integration over η we find

$$\frac{\partial}{\partial t}\langle\eta^{1/\mu_W}\rangle=\text{const}$$

or

$$\langle\eta^{1/\mu_W}\rangle=\text{const}\times t . \tag{7.9}$$

The formulas (7.9) give the necessary asymptotic behavior for $t\to\infty$, which also can be rewritten in the form

$$\langle\eta\rangle=\text{const}\times t^{\mu_W} \tag{7.10}$$

if the scaling law is used. The scaling law comes from the general expression (7.7) and had its origin in the self-similar structure of the Weierstrass random walk (7.1).

The final step can be carried out if we recall that η is an action and therefore $\eta\sim R^2$ where R is a particle displacement, so that from (7.10)

$$\langle R\rangle=\text{const}\times t^{\mu_W/2} . \tag{7.11}$$

Comparing (7.11) to (2.9) one gets

$$\mu=\tfrac{1}{2}\mu_W , \tag{7.12}$$

or from (6.9)

$$\mu=\ln(\delta\bar{I}_0)/2\ln\bar{T}_0 . \tag{7.13}$$

Using Table I we can put some appropriate values for $\bar{T}_0\sim 6.2$ and for $\delta\bar{I}_0\sim 14$. Then (7.13) gives $\mu\sim 0.72$ which is in good agreement with computations (see Fig. 3).

The main significance of the result (7.13) is that the exponent μ in the transport formulas (7.11) or (2.9) can be expressed through the local constants of the particle dynamics. One can expect the constant μ to be as universal as the constants $\delta\bar{I}_0$ and $\bar{T}_0$. We hope to come back to this issue elsewhere.

VIII. SPACE-TIME SCALES AND ERGODICITY

It was mentioned in [16] that existence of flights and self-similarity in particle dynamics can create serious difficulties in using the ergodic theorem. Here we can discuss this problem in more detail. A simple form of the ergodic theorem is the equality of the time and phase-space averages:

$$\lim_{t\to\infty}\frac{1}{t}\int_0^t f(x(t))dt=\langle f(x(t))\rangle=\langle f(x(0))\rangle\equiv f_0 , \tag{8.1}$$

where $x(t)$ is set of all dynamical variables, f is integrable function, and angular brackets $\langle\ \rangle$ mean averaging with invariant measure over the phase volume of a system.

The usual way to observe the property (8.1) is to find the time average and the phase average and to compare them. Phase averaging can be performed by observing, say, N orbits of the time extent t_N each. One can expect that if

$$Nt_N=t , \tag{8.2}$$

and t is fairly large, then the results for all three cases in (8.1) will be approximately the same. The last case in (8.1) corresponds to the only one orbit which can be considered either as N_1 pieces of the time extent t_{N_1} or as N_2 pieces of the time extent t_{N_2}. Self-similar transport raises new problems.

The questions are what is the time scale t_0 after which the left-hand side limit in (8.1) is sufficiently close to f_0, and what is the sufficient number of orbits N_0 that the phase-space averaging over the N_0 orbits is close to f_0? If N_0 and t_0 are known, then one can put $t=t_0$ in (8.2) and consider different possibilities with $N\geq N_0$. This scheme works fairly well if there is a good mixing property. In the case of the self-similar transport, the characteristic time t_0 for the time average can exceed any reasonable computational time and the scheme (8.2) does

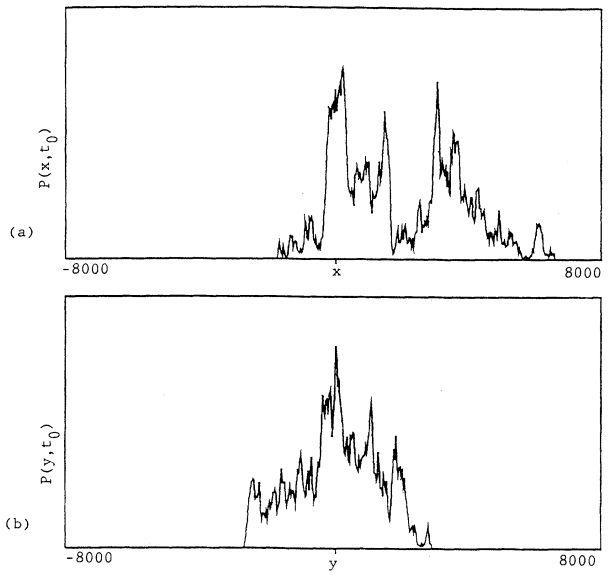

FIG. 10. Example of the displacements along x and y distribution function for one orbit of $t=10^8$ steps ($t=10^6$) and $\epsilon=2.9$.

not work. Unfortunately, from the point of view of the averaging, one long orbit of the time extent t, divided into N pieces, does not represent the same as averaging over N arbitrary orbits of the time extent t/N. Figure 10 shows the histogram of displacements for one orbit in the case of normal transport ($\mu=\frac{1}{2}$) with $t=10^8$ steps of computations or $t=10^6$ in the units in which the differential equations are written. Clearly even in this case long flights affect the distribution of displacements. The picture corresponds to the state which is far from the equilibrium whereas for 100 orbits of the time extent 10^4 one can get a picture similar to Figs. 4(a) and 4(b). This explains, in particular, how important the accuracy of computations is for the cases with flights, because errors of the roundoff and discretizations can influence the exponent in transport or the character of the distribution function. Absence of the characteristic time and space scales enhances this effect for a self-similar transport.

IX. FLIGHTS AND DISTRIBUTION FUNCTION

An orbit of a particle that carries out a random walk can be a mixture of different small pieces of almost regular motion. Any flight can be interpreted as a long piece of almost regular motion. The flights always exist in typical situations of dynamical chaos, but their measure is different for cases of anomalous or normal diffusion. Such a property may be visualized in the form of a particle position dependence on t: $x=x(t)$, $y=y(t)$. We set $x(t)=x_+(t)-x_-(t)$, where $x_+(t)$ and $x_-(t)$ are both continuous and

$$\dot{x}_+(t)=\begin{cases}\dot{x}(t), & \dot{x}>0\\ 0, & \dot{x}\le 0\end{cases}, \qquad \dot{x}_-(t)=\begin{cases}0, & \dot{x}\ge 0\\ -\dot{x}(t), & \dot{x}<0\end{cases}. \tag{9.1}$$

Equations (9.1) represent only monotonic changes of $x(t)$ in increasing (x_+) or decreasing (x_-) directions. This separation, usually carried out for functions of bounded variation, is a useful way to visualize a function with a great deal of oscillation, such as is manifest in Figs. 2(a)–2(c). The corresponding plots are given in Fig. 11 for the first 1000 steps. Each picture has three consecutive pieces of the initial part of an orbit. They represent $x^+(t)$ for the normal case [(a) and (c)] and anomalous one [(b) and (d)]. A flight in $x(t)$ has corresponding stagnation in $y(t)$ and vice versa. The flights are short and there is almost no serious difference between cases of $\epsilon=2.3$ and 2.9. The difference comes from the long-time observation and the long flights. Nevertheless, the phenomena of flights, even when they are short, creates a Poisson-like distribution function near the origin (see Figs. 4 and 5). We can relate this to the Poisson distribution of the Poincaré recurrence times which is also Poisson-like for not too large values of the recurrence times [23,45].

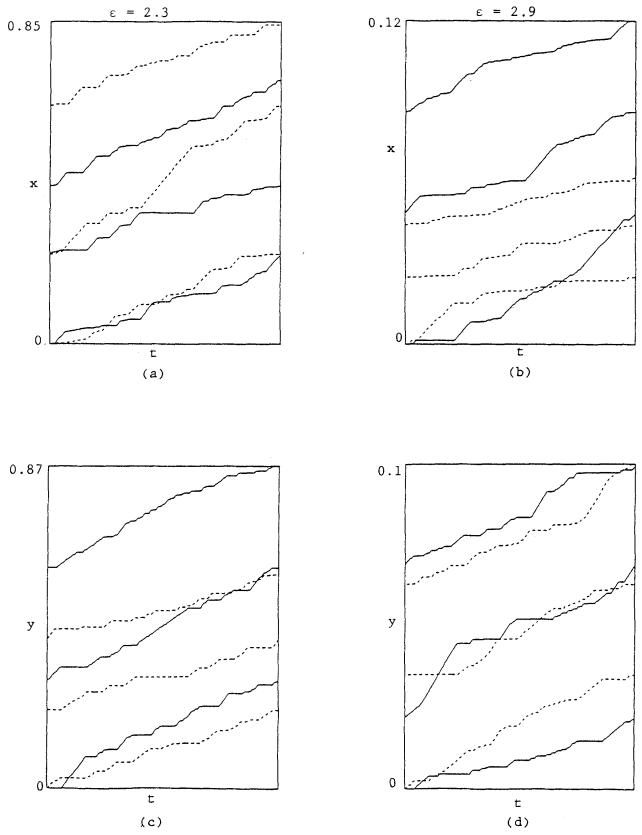

FIG. 11. Orbits represented in terms of functions of positive variation. (a) and (c) show fractal properties of single direction particle propagation for the anomalous case $\epsilon=2.3$ and (c) and (d) show the same for the normal case $\epsilon=2.9$. Solid curves correspond to x^+, y^+ and dashed curves correspond to x^-, y^-. The orbits are displayed in three pieces to show details better.

ACKNOWLEDGMENTS

This work was supported by the U.S. Department of Energy, Grants No. DE-FG02-86ER53223 and No. DE-FG02-92ER54184 and by the U.S. Department of the Navy, Grant No. N00014-93-1-0218.

[1] G. M. Zaslavsky and B. V. Chirikov, Usp. Fiz. Nauk. **101**, 3 (1972) [Sov. Phys. Usp. **14**, 549 (1972)].
[2] B. V. Chirikov, Phys. Rep. **52**, 264 (1979).
[3] A. B. Rechester and R. B. White, Phys. Rev. Lett. **44**, 1586 (1980).
[4] J. R. Cary and J. D. Meiss, Phys. Rev. A **24**, 2664 (1981).
[5] C. F. F. Karney, Physica D **8**, 360 (1983).
[6] I. Dana, N. W. Murray, and I. C. Percival, Phys. Rev. Lett. **62**, 233 (1989).
[7] A. Lichtenberg and M. A. Liberman, *Regular and Stochastic Motion* (Springer, New York, 1992).
[8] I. C. Percival, *Nonlinear Dynamics and Beam-Beam Interaction,* in Proceedings of the Symposium on Nonlinear Dynamics and Beam-Beam Interaction, AIP Conf. Proc. No. 57, edited by M. Month and J. C. Herrera (AIP, New York, 1979).
[9] S. Aubry, Physica D **7**, 240 (1983).
[10] V. I. Arnold, Dokl. Akad. Nauk SSSR **156**, 9 (1964) [Sov. Math. Dokl. **5**, 581 (1964)].
[11] G. M. Zaslavsky, M. Yu. Zakharov, R. Z. Sagdeev, D. A. Usikov, and A. A. Chernikov, Zh. Eksp. Teor. Fiz. **91**, 500 (1986) [Sov. Phys. JETP **64**, 294 (1986)].
[12] G. M. Zaslavsky, R. Z. Sagdeev, and A. A. Chernikov, Zh. Eksp. Teor. Fiz. **94**, 102 (1988) [Sov. Phys. JETP **67**, 270 (1988)].
[13] G. M. Zaslavsky, R. Z. Sagdeev, D. A. Usikov, and A. A. Chernikov, *Weak Chaos and Quasiregular Patterns* (Cambridge University Press, Cambridge, England, 1991).
[14] V. V. Beloshapkin, A. A. Chernikov, M. Ya. Natenzon, B. A. Petrovichev, R. Z. Sagdeev, and G. M. Zaslavsky, Nature (London) **337**, 113 (1989).
[15] A. A. Chernikov, B. A. Petrovichev, A. V. Rogalsky, R. Z. Sagdeev, and G. M. Zaslavsky, Phys. Lett. A **144**, 127 (1990).
[16] V. V. Afanas'ev, R. Z. Sagdeev, and G. M. Zaslavsky, Chaos **1**, 143 (1991).
[17] D. K. Chaikovsky and G. M. Zaslavsky, Chaos **1**, 463 (1991).
[18] M. Schwägerl and J. Krug, Physica D **52**, 143 (1991).
[19] B. A. Petrovichev, A. V. Rogalsky, R. Z. Sagdeev, and G. M. Zaslavsky, Phys. Lett. A **150**, 391 (1990).
[20] M. Ding, C. Grebogi, E. Ott, and J. A. York, Phys. Rev. A **42**, 7025 (1990).
[21] B. V. Chirikov and D. L. Shepelyansky, in *Renormalization Group,* edited by D. V. Shirkov, D. I. Kazakov, and A. A. Vladimirov (World Scientific, Singapore, 1988), p. 221.
[22] B. V. Chirikov, Chaos, Solitons and Fractals **1**, 79 (1991).
[23] G. M. Zaslavsky and M. Tippett, Phys. Rev. Lett. **67**, 3251 (1991).
[24] P. Lévy, *Théorie de l'Addition des Variables Aléatoires* (Gauthier-Vilars, Paris, 1937).
[25] B. Mandelbrot, *The Fractal Geometry of Nature* (Freeman, San Francisco, 1982).
[26] M. F. Schlesinger, B. J. West, and J. Klafter, Phys. Rev. Lett. **58**, 1100 (1987).
[27] E. Montroll and M. F. Shlesinger, in *Studies in Statistical Mechanics,* edited by J. Leibowitz and E. Montroll (North-Holland, Amsterdam, 1984), Vol. II, pp. 1–121.
[28] G. M. Zaslavsky, Fluid Dyn. Res. **8**, 127 (1991).
[29] M. F. Schlesinger, Annu. Rev. Phys. Chem. **39**, 269 (1988).
[30] H. Scher, M. F. Shlesinger, and J. T. Bendler, Phys. Today, **44** (1), 26 (1991).
[31] G. M. Zaslavsky, in *Topological Aspects of the Dynamics of Fluids and Plasmas,* edited by H. K. Moffatt, G. M. Zaslavsky, P. Comte, and M. Tabor (Kluwer, Boston, 1992).
[32] V. I. Arnold, C. R. Acad. Sci. Paris **261**, 17 (1965).
[33] D. Stevens, New York University, CIMS Report No. MF-104, 1985 (unpublished).
[34] G. D. Birkhoff, *Collected Mathematical Papers* (American Mathematical Society, New York, 1950), Vol. 2.
[35] V. I. Arnold, Sov. Math. Dokl. **2**, 247 (1961).
[36] J. D. Meiss, Phys. Rev. A **34**, 2375 (1986).
[37] D. F. Escande, Phys. Rep. **121**, 165 (1985).
[38] J. Meiss and E. Ott, Phys. Rev. Lett. **55**, 2741 (1985).
[39] J. Meiss and E. Ott, Physica D **20**, 387 (1986).
[40] B. D. Hughes, M. F. Shlesinger, and E. W. Montroll, Proc. Natl. Acad. Sci. U.S.A. **78**, 3287 (1981).
[41] G. M. Zaslavsky, *Chaos in Dynamic Systems* (Harwood Academic, New York, 1985).
[42] G. H. Hardy, Trans. Am. Math. Soc. **17**, 301 (1980).
[43] M. V. Berry and Z. V. Lewis, Proc. R. Soc. London, Ser. A **370**, 459 (1980).
[44] B. D. Hughes, E. W. Montroll, and M. F. Shlesinger, J. Stat. Phys. **28**, 111 (1982).
[45] B. V. Chirikov and D. L. Shepelyansky, Physica D **13**, 395 (1984).